4810 J. Med. Chem. 2009, 52, 4810–4819
DOI: 10.1021/jm900314j

Journal of Medicinal Chemistry Article

Identification of Inhibitors of Checkpoint Kinase 1 through Template Screening

Thomas P. Matthews,[†] Suki Klair,[§] Samantha Burns,[†] Kathy Boxall,[†] Michael Cherry,[§] Martin Fisher,[§] Isaac M. Westwood,[‡] Michael I. Walton,[†] Tatiana McHardy,[†] Kwai-Ming J. Cheung,[†] Rob Van Montfort,[‡] David Williams,[§] G. Wynne Aherne,[†] Michelle D. Garrett,[†] John Reader,[§] and Ian Collins*[,†]

[†]*Cancer Research UK Centre for Cancer Therapeutics and* [‡]*Sections of Cancer Therapeutics and Structural Biology, The Institute of Cancer Research, 15 Cotswold Road, Sutton, Surrey SM2 5NG, U.K., and* [§]*Sareum Ltd, 2 Iconix Park, Pampisford, Cambridge CB22 3EG, U.K.*

Received March 12, 2009

Checkpoint kinase 1 (CHK1) is an oncology target of significant current interest. Inhibition of CHK1 abrogates DNA damage-induced cell cycle checkpoints and sensitizes p53 deficient cancer cells to genotoxic therapies. Using template screening, a fragment-based approach to small molecule hit generation, we have identified multiple CHK1 inhibitor scaffolds suitable for further optimization. The sequential combination of in silico low molecular weight template selection, a high concentration biochemical assay and hit validation through protein−ligand X-ray crystallography provided 13 template hits from an initial in silico screening library of ca. 15000 compounds. The use of appropriate counter-screening to rule out nonspecific aggregation by test compounds was essential for optimum performance of the high concentration bioassay. One low molecular weight, weakly active purine template hit was progressed by iterative structure-based design to give submicromolar pyrazolopyridines with good ligand efficiency and appropriate CHK1-mediated cellular activity in HT29 colon cancer cells.

Introduction

The genomic integrity of replicating cells is maintained by a network of sensors that monitor DNA and control ordered progression through the cell cycle. In response to DNA damage, this network serves to activate checkpoints at various stages of the cell cycle that delay progression, allowing cells to repair the damage or directing them to programmed cell death if the damage is too severe.[1,2] Many well established cancer chemotherapies and radiotherapy exert their therapeutic effect through damage to DNA. The activation of cell cycle checkpoints provides an opportunity for cancer cells, as well as normal cells, to repair DNA damage and therefore reduce the effect of, or become resistant to, DNA-damaging treatments.[3] The G1 checkpoint mediated by p53 is a major barrier to genomic instability, but over half of all cancers are functionally defective for the p53 pathway.[4] These tumor cells are more reliant on the S and G2/M checkpoints to repair damage. Therefore drugs that abrogate the DNA damage-induced S and G2/M checkpoints should selectively sensitize p53 deficient cancer cells to genotoxic cancer therapies.[3,5−7]

Checkpoint kinase 1 (CHK1[a]) is a serine/threonine kinase that is phosphorylated and activated by the upstream kinase ataxia-telangiectasia mutated and rad3-related (ATR) in response to DNA damage. ATR itself is activated by DNA damage or replication stress that causes double- or single-strand breaks in DNA, initiating a signaling cascade culminating in cell cycle arrest in the S and G2/M phase.[8,9] Activated CHK1 signals to several proteins to bring about cell cycle arrest, in particular the CDC25 family of phosphatases. CDC25 phosphatases are essential to dephosphorylate and activate the cyclin dependent kinase (CDK)/cyclin complexes that drive cell cycle progression. CHK1-mediated-phosphorylation of the CDC25 proteins has been shown to block their ability to dephosphorylate CDKs, through inhibiting the direct interaction of CDC25 proteins with CDKs, sequestration in the cytoplasm, or ubiquitin-mediated degradation, thus leading to cell cycle arrest.[10] Because cells lacking intact p53-dependent G1 checkpoints are particularly reliant on S and G2/M checkpoints, they are more sensitive to chemotherapeutic treatment in the presence of a CHK1 inhibitor.[7] Inhibition of CHK1 by siRNA[5,11,12] or small molecules[7,13−20] has been shown to abrogate cell cycle arrest, leading to premature mitotic entry and enhanced tumor cell death following DNA damage by a range of chemotherapeutics. In particular, a number of ATP-competitive inhibitors of CHK1 have been shown to sensitize tumors to DNA-damaging agents in preclinical animal models[18−21] and ATP-competitive CHK1 inhibitors are now in phase I clinical trials.[19−22]

Several distinct chemotypes have been identified as CHK1 inhibitors, and these have been extensively reviewed[14,21−23] (Chart 1). A collection of scaffolds have been developed based on the indolocarbazole natural product kinase inhibitor staurosporine and its analogue UCN-01.[24] Most other published CHK1 inhibitors originate from hits discovered by high throughput screening (HTS) of large conventional compound libraries.[15−17] In some cases, HTS was combined with preliminary in silico screening to reduce the size of the biochemical screen and enhance the hit rate.[25,26] The development of

*To whom correspondence should be addressed. Phone +44 208 7224317. Fax: +44 208 7224126. E-mail: ian.collins@icr.ac.uk.

[a] Abbreviations: AlphaScreen, amplified luminescent proximity homogeneous assay screen; ATR, ataxia-telangiectasia mutated and rad3-related; CDK, cyclin dependent kinase; CHK1, checkpoint kinase 1; HTS, high throughput screening; LE, ligand efficiency.

 Published on Web 07/02/2009

Chart 1. Structures of Selected Published Clinical Candidate CHK1 Inhibitors

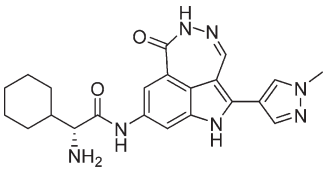

PF-00477736[19]

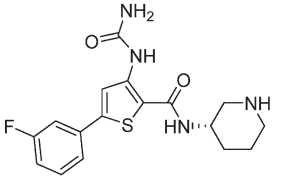

AZD7762[20]

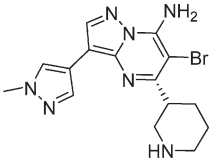

SCH-900776[45]

small molecule CHK1 inhibitors from these sources has been aided by the availability of the X-ray crystal structure of the enzyme[27] and protein−ligand complexes.[15−17]

Fragment-based screening offers an alternative approach for small molecule hit generation.[28] A potential benefit of fragment screening is that chemical diversity space can be probed effectively using a smaller number of molecules than is possible with conventional HTS libraries. Low molecular weight fragments may have weak binding affinities, outside the range of conventional biochemical assays, necessitating the use of biophysical screening techniques (NMR, X-ray crystallography, or surface plasmon resonance) to detect interactions with the target protein. Despite the low affinity of the fragment hits, they are often bound with high ligand efficiency (LE) and thus serve as good platforms for elaboration to more potent ligands.[29] Structural data on the binding mode of the fragments is essential, however, if the weak initial hits are to be progressed rapidly to tractable lead compounds. We have used a template-based approach to identify new inhibitors of CHK1, which balances the efficiency of a biochemical assay for screening compound activity with the desirability of starting with small, ligand-efficient structures to maximize the probability of developing a "druglike" inhibitor during optimization. The templates are therefore low molecular weight structures, which are large enough to have detectable binding at high micromolar levels in a high concentration biochemical assay yet small enough to benefit from the higher coverage of diversity space offered by fragments.[30] Hits from the high concentration CHK1 kinase assay were validated by crystallography of the bound complex to provide the necessary structural information, enabling progression to more potent inhibitors.

Results and Discussion

The structural features and calculated physicochemical parameters used to select the template screening set in this work are outlined in Table 1. In general, these cover the

Table 1. Properties Defining the Templates

property	template values
no. of heavy atoms	8−24
CLogP	−2 to 4
total H-bond donors and acceptors	1−6
rotatable bonds	0−6
no. of rings	1−3

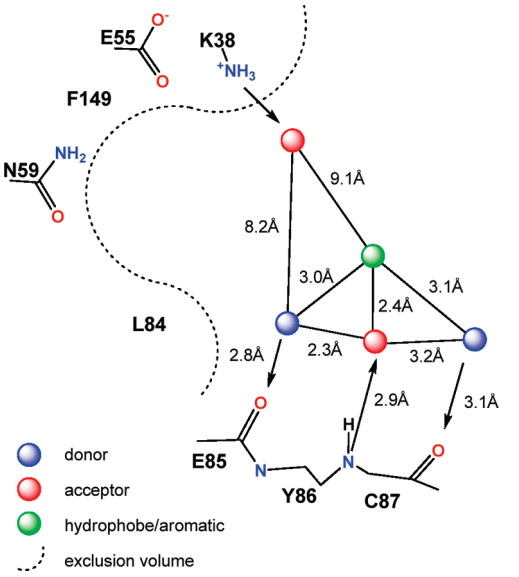

Figure 1. CHK1 ATP-binding site pharmacophore used for the virtual screen of commercially available templates.

overlap between the property space proposed for fragment libraries employed in biophysical screening and that proposed for "leadlike" compounds in HTS.[31] The upper limits to size, lipophilicity, and functional group count allow for addition of atoms during lead optimization while still remaining in "druglike" chemical space. Approximately 15000 templates were identified from commercially available compound collections using these library filters. To select appropriate templates for biochemical screening, a pharmacophore search was performed using the pharmacophore tools within MOE (Chemical Computing Group)[32] to identify compounds with the features of potential kinase inhibitors.

Template structures were matched to five conserved features within the kinase ATP site in its active conformation, as illustrated in Figure 1. The query was built from an overlay of the structure of multiple published ligands in CHK1 using a combination of the protein and ligand structures to define the position of the pharmacophore points. A match to at least three of the five points defined was required to warrant a hit. Volume constraints were also applied to limit the scope of the search, with the intent of reducing the number of false positives identified in the pharmacophore search. To allow for some leeway in movement of individual protein residues, exclusion volume spheres defined by radii of 2.0 Å were placed at each of the protein heavy atom positions surrounding the ATP-binding site in the structure of CHK1 (PDB 1IA8). These volumes were amalgamated into a single volume definition, and molecules were rejected if an atom from the pharmacophore-matching pose fell within the excluded volume. Hits from the search were clustered by structural type, focusing on the core rings of each compound, and representatives from each cluster were chosen by visual inspection. In total, 361 templates were selected for biochemical screening.

The focused set of 361 compounds was evaluated in a 384-well format Amplified Luminescent Proximity Homogeneous Assay Screen (AlphaScreen)[33] for inhibition of CHK1 kinase activity, measured by the reduction in phosphorylation of a CHK1 substrate peptide. The assay was adapted for screening at high ligand concentration (250 μM), with each test plate run under three different conditions. First, compounds were tested six times in the standard AlphaScreen format to achieve a high level of confidence. The screen was then run in triplicate with the inclusion of a detergent (0.01% Triton X) to eliminate potential false positives due to aggregation of poorly soluble compounds at the high concentration.[34] Finally, the plates were counterscreened three times in the presence of phosphorylated substrate peptide to eliminate compounds interfering with the AlphaScreen signal. False positives in AlphaScreen assays have been observed due to compound fluorescence or reaction with the singlet oxygen generated in the screen.[35]

Two levels of hits were classified from this screening data. The first set of compounds selected inhibited CHK1 activity by more than 25% at 250 μM in at least 5/6 of the replicate AlphaScreen assays and retained this activity in at least 2/3 of the assays in the presence of detergent. Compounds were not classified as hits if apparent inhibition was observed in the presence of phosphorylated peptide. This identified nine high-confidence hits showing inhibition of CHK1 between 35 and 79% at 250 μM. To maximize the potential output from the screen, 13 further compounds were selected that inhibited CHK1 by more than 25% at 250 μM in at least 3/6 of the multiple assay runs while not giving inhibition in the assay interference counter screen, but showed some reduction in activity when assayed in the presence of detergent.

The 22 template hits from the bioassay were validated using X-ray crystallography by soaking into crystals of the apo-CHK1 kinase domain. Hits were grouped by structural classes, and where a group contained several compounds, representative members were selected for crystallography. Soaking experiments were therefore set up with eight of the high confidence hits and seven of the lower confidence hits. From these 15 chemically diverse structures, nine (**1**−**9**) were confirmed to bind in the ATP-binding site of CHK1 by X-ray crystallography (Chart 2, Table 2). The final hit-rate of the screen was approximately 0.06% from the virtual template set (2.5% from the 361 assayed compounds). The overall screening cascade is summarized in Figure 2. Importantly, the validation rate by crystallography was much greater for the high confidence hits than for the lower confidence compounds that showed a reduction in activity when assayed in the presence of detergent. Of the nine high confidence hits, soaking experiments were carried out with eight distinct chemotypes, of which seven were confirmed by crystallographic analysis (compounds **3**−**9**). In contrast, of the 13 lower confidence hits, seven distinct chemotypes were selected for X-ray crystallography but only two compounds, **1** and **2**, were confirmed as ATP-competitive binders to CHK1. This supports the application of counter screens for potential compound aggregation to increase the useful output of low affinity, high concentration screens of this type. Although the hit **2** was found to bind in the ATP-binding site of CHK1, this compound failed to show CHK1 inhibition at high concentration in a DELFIA-based kinase assay developed to support medicinal chemistry progression of the compounds (Table 2). Thus the significantly lower activity of **2** recorded in the AlphaScreen in the presence of detergent is more representative of the targeted biological potency of the compound. In contrast, the biological activities of the high confidence hits **5**−**9** in the initial screens were all confirmed in the second assay format.

Chart 2. Chemical Structures of the Nine Template Hits Validated by CHK1 Crystallography[a]

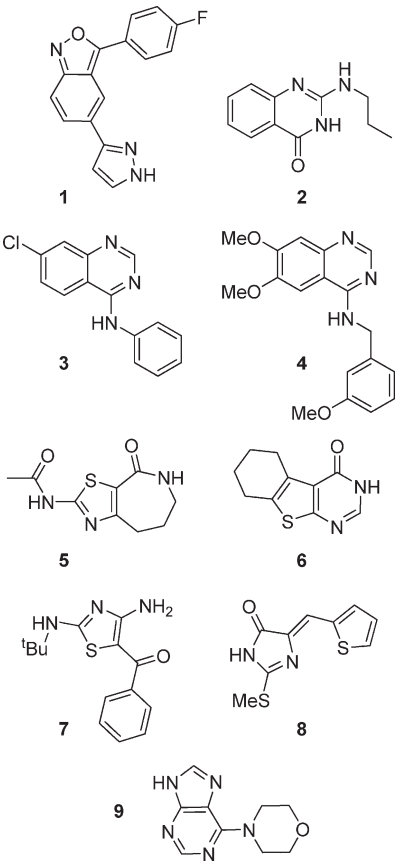

[a] Compounds **1** and **2** were lower confidence hits from the bioassay, which showed some nonspecific inhibition, while compounds **3**−**9** were high confidence hits that showed similar activity in the presence and absence of Triton X-100 detergent in the bioassay.

Table 2. CHK1 Inhibition by Crystallographically Validated Template Hits **1**−**9** in High Concentration AlphaScreen and DELFIA Assays

crystallographically validated hits	AlphaScreen % inhibition at 250 (±SD) μM[a]	AlphaScreen +0.01% Triton-X100 (% inhibition at 250 μM ± SD)[b]	DELFIA (% inhibition at 100 μM)[c]
1	26.4 (±6.9)	6.5 (±3.2)	nd
2	40.9 (±8.4)	14.2 (±3.3)	0%
3	41.9 (±2.5)	41.5 (±1.7)	nd[d]
4	50.1 (±5.0)	52.8 (±1.1)	nd
5	51.4 (±1.2)	43.1 (±3.0)	27%
6	38.5 (±3.2)	45.3 (±1.6)	IC_{50} = 52 μM (46, 57)[e]
7	36.9 (±1.7)	39.9 (±4.5)	33%[e]
8	35.7 (±1.3)	33.5 (±12.8)	32%
9	75.7 (±1.0)	63.0 (±0.7)	IC_{50} = 42 μM (28, 58)[e]

[a] Mean (±SD) for $n = 6$ determinations. Positive control staurosporine gave 73 (±9.9) % inhibition @ 25 nM. [b] Mean (±SD) for $n = 3$ determinations. Positive control staurosporine gave 73 (±15) % inhibition @ 25 nM. [c] Single determination. Standard inhibitor staurosporine gave IC_{50} = 2.1 (±1.8) nM. [d] nd = not determined. [e] Mean of 2 independent determinations, individual values in parentheses.

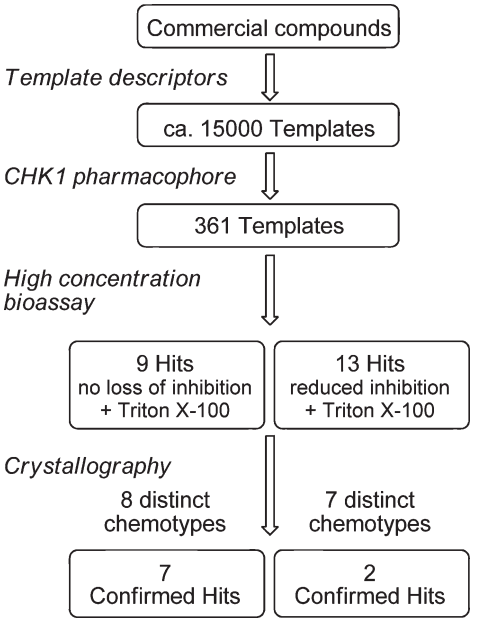

Figure 2. Summary of the template screening cascade and hit validation.

All nine validated hits bound in the ATP pocket. However, the core structures, binding modes and degree of hydrogen bonding to the kinase hinge region, varied. Templates **1**–**4** showed only weak, single hydrogen bond contacts to the hinge region despite the presence of multiple hydrogen-bond donors and acceptors in the molecules. In contrast, templates **5**–**9** were more firmly anchored in the binding site with bi- or tridentate hydrogen bonding to the hinge region. These latter hits were considered more promising as the presence of stronger polar interactions to the starting template should reduce the chance of encountering major changes to the binding mode during the elaboration of the inhibitors.[36] The CHK1 crystal structures of five of these validated hits, **5**–**9**, are shown in Figure 3. A structural overlay of the hits shows that they occupied similar space relative to the hinge region of the kinase (Figure 3F). The thiazolo[5,4-*c*]azepin-4-one **5** adopted a bidentate hinge-binding pose, with the lactam forming hydrogen bonds to the backbone amides of Glu85 and Cys87 in CHK1 (Figure 3A). The core of **5** occupied the cleft of the ATP-binding site with the pendant acetamide substitutent located close to Glu91 on the solvent-exposed specificity surface. The tricycle **6** also adopted a bidentate hinge-binding pose, with two hydrogen bonds from the pyrimidinone functionality to Glu85 and Cys87 (Figure 3B). The pyrimidinone was also hydrogen-bonded through a neighboring water molecule to the side chain of Ser147. The water molecule was situated at the mouth of a highly conserved interior pocket of CHK1 defined principally by residues Val68, Asn59, and Glu55 in which a trio of water molecules is typically observed.[37] The remainder of the tricycle was directed toward the solvent with the cyclohexane located near the specificity surface formed by residues Gly89, Gly90, and Glu91. Unique among this set of hits, the aminothiazole **7** bound to the hinge region in a tridendate manner with the primary amine hydrogen-bonding to Glu85, and the thiazole nitrogen and *tert*-butyl substituted amine to the amino and carbonyl functionality of Cys87, respectively (Figure 3C). The phenyl ketone of **7** was pointed into the ribose-binding pocket, while the *tert*-butylamino group

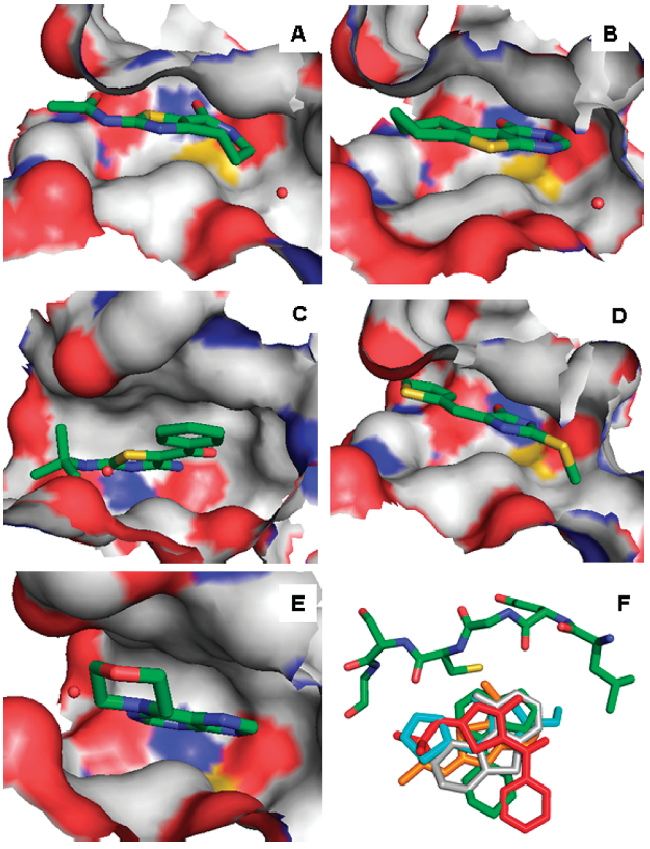

Figure 3. Crystal structures of hits **5** (A), **6** (B), **7** (C), **8** (D), and **9** (E) in the ATP binding pocket of CHK1. Panel F: Overlay of hits **5**–**9** relative to the hinge-region of CHK1, orange = **5**, gray = **6**, red = **7**, cyan = **8**, green = **9**.

emerged from the ATP-site near the specificity surface. The cocrystal structure of **8** bound to CHK1 showed bidentate hydrogen bonding between the imidazolone motif of the ligand and the backbone amides of Glu85 and Cys87 (Figure 3D). The pendant thiophene was directed over the specificity surface toward solvent, while the thiomethylether pointed toward the water-filled pocket within CHK1. The initial elaboration of the purine **9**, which binds in the ATP site of CHK1 (Figure 3E) and has an IC_{50} of 42 μM and a calculated LE = 0.42 kcal mol^{-1} heavy atom^{-1}, is discussed below as an example of several weakly active but ligand efficient template hits from this screen that were progressed to more potent CHK1 inhibitors using structure-based drug design.

The crystal structure of 4-(9*H*-purin-6-yl)morpholine **9** bound to CHK1 confirmed the expected hydrogen bonds between N-3 and N-9 of the purine with the backbone amides of Cys87 and Glu85, respectively (Figure 4A). This binding mode has been reported for other purine-derived kinase inhibitors.[38,39] Importantly, this is not equivalent to the binding of the purine moiety of ATP or ADP, where the heterocycle is in a very different orientation, with hydrogen bonding to the hinge region from N-1 of the purine and a 6-NH_2 substituent. The morpholine substituent of **9** did not appear to make specific contacts with the protein backbone but extended toward the ribose pocket. A limited number of analogues containing small polar side chains at C-2 or C-3 directed toward the ribose pocket were synthesized, including carboxylic acid, *N*-(*tert*-butyloxycarbonyloxy)amine, and amine groups. From these, the racemic morpholine analogue

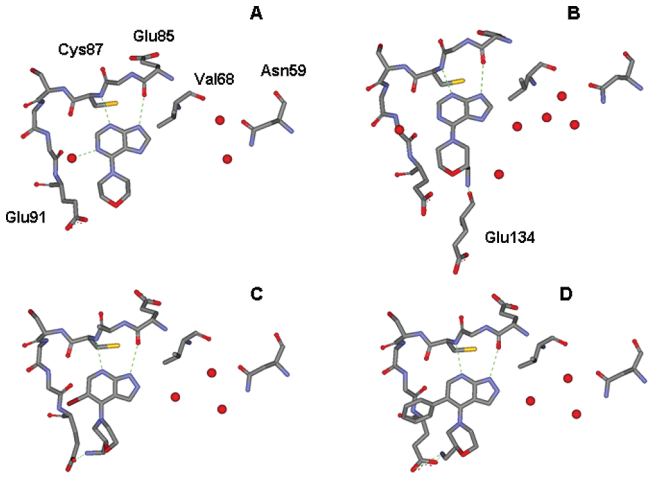

Figure 4. Details of the binding of **9** (A), **10** (B), **12** (C), and **14** (D) to CHK1 kinase domain. Residues and side chains not involved in binding are omitted for clarity. Water molecules detected in the interior pocket of CHK1 or hydrogen bonded to the inhibitors are shown as red spheres. Hydrogen bonds to the inhibitors are shown as dashed green lines.

10 bearing a methylamino group at C-2 gave increased potency and maintained LE relative to the hit (**10**, LE = 0.42 kcal mol^{-1} heavy atom^{-1}) (Table 3). A crystal structure confirmed the purine remained as the hinge binding component, while the pendant primary amine formed a network of polar interactions in the ribose pocket of CHK1 (Figure 4B). The amine bound directly to the backbone carbonyl of Glu134 and interacted with the side chains of Asn135 and Ser147 mediated by a water molecule. The amine was also close (ca. 3.4 Å) to the terminal carboxylate of Glu91.

We sought to alter the purine heterocyclic core at an early stage to explore novel inhibitors that retained the key nitrogens atoms to interact with the hinge region while providing new substitution vectors to explore additional regions of the binding site. Comparison of the crystal structures of the purines **9** and **10** with the structures of the other template hits **5**−**8** indicated that the purines lacked a substitution vector toward the kinase specificity surface (Figure 3F). This was introduced through switching to the pyrazolopyridine scaffold, resulting initially in the more potent ester **11**. Although pyrazolopyridines are well-known as kinase inhibitor scaffolds,[46] the introduction of the 4-(2-aminomethylmorpholin-4-yl) substituent led to novel compounds.[47] The reduced LE of **11** was recovered when the ester was replaced by a 5-bromo substituent to give **12**. The crystal structure of **12** showed a change in the orientation and conformation of the morpholine ring to deliver the pendant amine for direct interaction with the carboxylate of Glu91 (Figure 4C). The morpholine adopted a twisted conformation with respect to the plane of the bicycle as a result of a steric clash with the 5-bromo substituent. A possible weak interaction with a water molecule at the edge of the interior pocket was also detected (ca. 3.5 Å).

Substitution at C-5 of the pyrazolopyridine by thiophene (**13**) or phenyl (**14**) retained the submicromolar activity and acceptable LE. The crystal structure of **14** showed the morpholine ring adopting a near-identical conformation to that observed in **12** but with the pendant phenyl adopting a torsion of ca. 56°. In refining the structures of racemic **10**, **12**, and **14**, it was generally possible to obtain a reasonable fit for either enantiomer of the morpholine side chains to the observed electron density by changes to the conformation of the ring.

Table 3. Biological Activities and Ligand Efficiencies of Analogues of the Template Hit **9**

Structure	CHK1 inhibition IC_{50} (μM)[a]	LE (kcal mol^{-1} non-H atom^{-1})
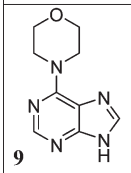 **9**	42 (28, 58)	0.42
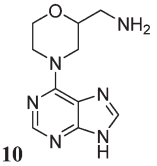 **10**	9.2 (7.0, 11)	0.42
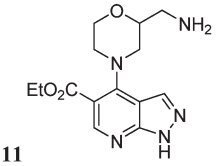 **11**	1.2[b]	0.39
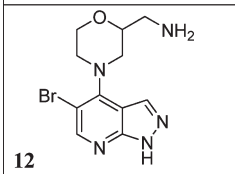 **12**	0.39 (0.33, 0.45)	0.52
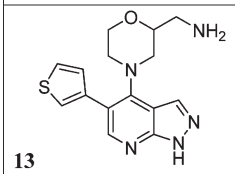 **13**	0.29[b]	0.43
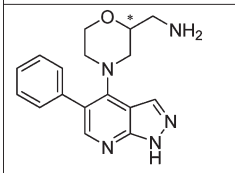 ***Rac*-14** **(*R*)-14** **(*S*)-14**	0.89 (0.85, 0.93) 0.70 (0.52, 0.88) 0.86 (0.72, 0.99)	0.38

[a] Mean of 2 independent determinations in DELFIA format, individual values in parentheses. Standard inhibitor staurosporine gave IC_{50} = 2.1 (±1.8) nM. [b] Single determination.

The single enantiomers of **14** were synthesized and tested but showed no appreciable enantiodiscrimination for binding to CHK1, emphasizing the conformational flexibility of the 2-aminomethylmorpholine.

The pyrazolopyridines were profiled for selectivity and cellular activity (Table 4). Some selectivity was seen for inhibition of CHK1 over the unrelated checkpoint kinase CHK2 (8−60-fold). The possible difference in therapeutic outcome of dual CHK1 and CHK2 inhibition, as opposed to selective CHK1 inhibition, remains to be determined. siRNA studies suggest that the CHK1 inhibitor phenotype dominates and is not necessarily enhanced by the simultaneous

Table 4. Selectivity and Cellular Data for Selected Compounds

no.	CHK1[a] IC_{50} (μM)	CHK2[b] IC_{50} (μM)	CDK1[c] % inhibition at 100 μM	abrogation of G2 check point[d] IC_{50} (μM)	96 h SRB[e] GI_{50} (μM)
11	1.2	74	3	19 (17, 20)	64 (60, 68)
12	0.39 (0.33, 0.45)[f]	7.4	37	5 (3.9, 6)	16 (14, 18)
13	0.29	4.6	48	6 (7, 5)	10.5 (10, 11)
***R*-14**	0.70 (0.52, 0.88)[f]	5.9	43	> 50	40[g]

[a] Single determination in DELFIA format. Standard inhibitor staurosporine gave IC_{50} = 2.1 (±1.8) nM. [b] Single determination in DELFIA format. Standard inhibitor staurosporine gave IC_{50} = 27 (±8) nM [c] Single determination in DELFIA format. Standard inhibitor staurosporine gave IC_{50} = 18 (±4) nM [d] Mean of 2 independent determinations in HT29 cells treated with etoposide to induce G2/M arrest, individual values in parentheses. Standard inhibitor staurosporine gave IC_{50} = 0.0017 (±0.0004) μM. [e] Mean of 2 independent determinations in HT29 cells, individual values in parentheses. Assay standard etoposide gave GI_{50} = 0.73 (±0.13) μM. [f] Mean of 2 independent determinations, individual values in parentheses. [g] single determination.

inhibition of CHK2.[11] Compounds **11**−**14** showed little inhibition of the cell cycle kinase CDK1. This is important for the interpretation of cellular checkpoint abrogation assays as inhibition of CDK1 will lead to interruptions in the cell cycle, independent of CHK1-mediated effects.[40] The compounds were assessed in $p53^{-/-}$ HT29 colon cancer cells for their ability to abrogate the G2-M checkpoint arrest induced by treatment with etoposide. HT29 and certain other $p53^{-/-}$ colon cancer cell lines have been shown to have increased sensitivity to CHK1 inhibitors in vitro and in vivo.[41] Compounds **11**−**13** abrogated the G2-M checkpoint in HT29 cells at concentrations 10−20-fold above the CHK1 inhibitory IC_{50} values. These compounds were also active in the growth inhibition assay, with some 2−3-fold selectivity for the CHK1-mediated cellular effect over general cytotoxicity. The phenyl substituted analogue (***R***)-**14** did not show similar cellular activity, with no abrogation of the G2-M checkpoint detectable. We speculate that this might reflect undetermined off-target activities of the compound and underlines the importance of measuring cellular activity as well as inhibition of target biochemical activity in the progression of hits.

Conclusions

We have shown that the template screening strategy described above is an effective means to generate new inhibitors of the checkpoint kinase CHK1. The combination of in silico template design, a high concentration AlphaScreen biochemical assay for primary hit detection, followed by confirmation using protein−ligand X-ray crystallography provided multiple validated template hits. This proved an attractive hit generation approach for CHK1 and is likely to be more widely applicable for other targets for which a robust high concentration bioassay is available. Our data reinforces the value of appropriate counter-screening to rule out nonspecific aggregation by test compounds in the high concentration bioassay. Although some poorly active templates can indeed be valid hits, and weak activity is expected for molecules in this molecular weight range, a much better validated hit rate was observed from those primary hits where no nonspecific inhibitory effect was detected. We have shown the rapid progression of one purine template hit using the initial structural information to give a more potent inhibitor and the subsequent application of iterative structure-based design to quickly generate submicromolar pyrazolopyridine inhibitors with good ligand efficiency. The pyrazolopyridine core possesses substitution patterns that should allow access to the key regions in CHK1 that are associated with highly specific inhibition. Although the pyrazolopyridines represent early stage leads, the compounds have appropriate CHK1-mediated cellular activity and successfully abrogate the G2-M checkpoint HT29 colon cancer cells. This demonstrates the ability of the template screen to efficiently identify progressible hit matter suitable for further optimisation.

Scheme 1[a]

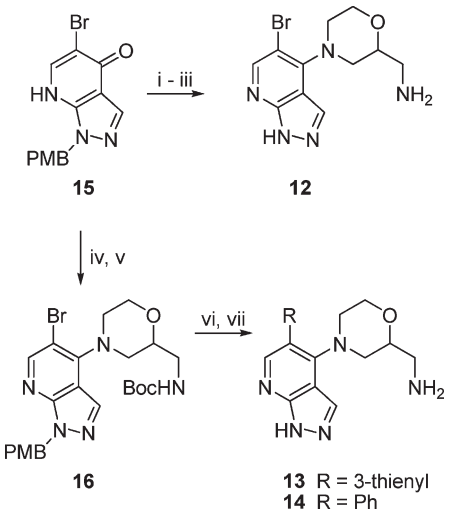

[a] Reagents and conditions: (i) $POCl_3$, 110°C; (ii) *tert*-butyl morpholin-2-ylmethylcarbamate, Et_3N, *n*-BuOH, 100°C (53% over 2 steps); (iii) 4M HCl−dioxane, rt (8%); (iv) $POCl_3$, 60°C (79%); (v) *tert*-butyl morpholin-2-ylmethylcarbamate, Et_3N, *n*-BuOH, 100°C (49%); (vi) $ArB(OH)_2$, $Pd(dppf)Cl_2$, Na_2CO_3, H_2O, MeCN, 140°C, microwave; (vii) CF_3CO_2H, 40°C (16−41% over 2 steps).

Experimental Section

Synthetic Chemistry. (4-(9*H*-Purin-6-yl)morpholin-2-yl)-methanamine (**10**) was prepared by direct nucleophilic aromatic substitution of 6-chloropurine with commercially available racemic *tert*-butyl morpholin-2-ylmethylcarbamate, followed by acid deprotection. Compound **11** was prepared from ethyl 4-chloro-1*H*-pyrazolo[3,4-*b*]pyridine-5-carboxylate[42] in a similar manner. The pyrazalopyridine bicyclic core was prepared from paramethoxybenzyl protected pyrazolopyridone **15** as previously described by Misra[43] (Scheme 1). Chlorination of **15** using phosphorus oxychloride at 110 °C also removed the paramethoxybenzyl group, and introduction of the morpholin-2-ylmethylamine by S_NAr displacement followed by deprotection yielded **12**. An advanced intermediate **16** with the paramethoxybenzyl protecting group still intact was formed by lowering the temperature of the chlorination step to 60 °C, followed by nucleophilic substitution as before. Suzuki couplings to the protected 5-bromopyrazolopyridine **16**, followed by dual deprotection by stirring overnight at 40 °C in trifluoroacetic acid, gave the thienyl and phenyl substituted compounds **13** and **14**.

tert-Butyl morpholin-2-ylmethylcarbamate was prepared as either enantiomer starting from the appropriate 3-amino-1, 2-propanediol **17** as described by Brenner et al.[44] (Scheme 2). For example, the 2-hydroxymethylmorpholine **18**[44] was *O*-tosylated. Displacement of the tosylate by azide, reduction, and protection of the primary amine gave the bis-carbamate **19**. Selective deprotection of the secondary amine was achieved by exposure to acid at low temperature (5 °C) to give **20**, from which the

Scheme 2[a]

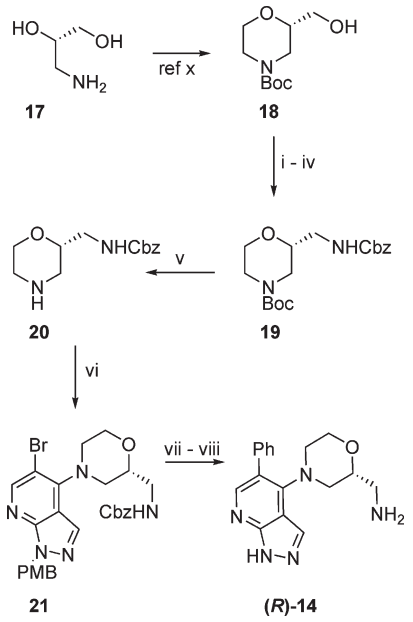

[a] Reagents and conditions: (i) TsCl, Et_3N, DMAP, CH_2Cl_2, 0°C → rt (85%); (ii) NaN_3, DMF, 80°C; (iii) $NH_4^+HCO_2^-$, Pd/C, MeOH, rt; (iv) Cbz-Cl, Et_3N, CH_2Cl_2, rt (42% over 3 steps); (v) 4M HCl-dioxane, 0°C → 5°C (83%); (vi) 5-bromo-4-chloro-1-(4-methoxybenzyl)-1*H*-pyrazolo[3,4-*b*]pyridine, Et_3N, *n*-BuOH, 160°C, microwave (67%); (vii) $PhB(OH)_2$, $Pd(dppf)Cl_2$, Na_2CO_3, H_2O, MeCN, 140°C, microwave (48%); (viii) CF_3CO_2H, 40°C (55%).

synthesis followed a similar path to that for the racemate. The intermediate **20** was reacted with 5-bromo-4-chloro-1-(4-methoxybenzyl)-1*H*-pyrazolo[3,4-*b*]pyridine to give the coupled product **21**. Suzuki coupling to **21** and double *N*-deprotection with trifluoroacetic acid gave ***R*-14**. The *S*-enantiomer of **14** was prepared in similar fashion.

General Synthetic Chemistry. Reactions were carried out under N_2. Organic solutions were dried over $MgSO_4$ or Na_2SO_4. Starting materials and solvents were purchased from commercial suppliers and were used without further purification. Microwave reactions were carried out using a Biotage Initiator 60 microwave reactor. Flash silica chromatography was performed using Merck silica gel 60 (0.025−0.04 mm). Ion exchange chromatography was performed using Isolute Flash SCX-II (acidic) or Flash NH2 (basic) resin cartridges. ^{1}H NMR spectra were recorded on a Bruker AMX500 instrument using internal deuterium locks. Chemical shifts (δ) are reported relative to TMS (δ = 0) and/or referenced to the solvent in which they were measured. Combined HPLC−MS analyses were recorded using a Waters Alliance 2795 separations module and Waters/Micromass LCT mass detector with electrospray ionization (+ve or −ve ion mode as indicated) and with HPLC performed using Supelco DISCOVERY C18, 50 mm × 4.6 mm or 30 mm × 4.6 mm i.d. columns, at a temperature of 22 °C with gradient elution of 10−90% MeOH/0.1% aqueous formic acid at a flow rate of 1 mL/min and a run time of 6 min. Compounds were detected at 254 nm using a Waters 2487 dual λ absorbance detector. All tested compounds gave ≥95% purity as determined by this method. All purified synthetic intermediates gave ≥95% purity as determined by this method except where indicated in the text. High-resolution mass spectra were measured on an Agilent 6210 ToF HPLC−MS with a Phenomenex Gemini 3 μm C18 (3 cm × 4.6 mm i.d.) column.

(4-(9*H*-Purin-6-yl)morpholin-2-yl)methanamine (10). A solution of *tert*-butyl morpholin-2-ylmethylcarbamate (0.115 g, 0.53 mmol), 6-chloro-9*H*-purine (0.035 g, 0.23 mmol), and Et_3N (0.058 mL, 0.42 mmol) in NMP (1.1 mL) was heated in a microwave reactor at 140 °C for 2 × 5 min. The solvent was removed in vacuo, and the residue was purified by preparative HPLC to afford *tert*-butyl(4-(9*H*-purin-6-yl)morpholin-2-yl) methylcarbamate (0.035 g, 0.10 mmol, 46%). LC−MS *m*/*z* 357 (M + Na^+), R_t = 2.05 min. ^{1}H NMR (MeOH-d_4) δ 1.48 (9H, s), 3.02 (1H, t, *J* = 12.0 Hz), 3.26 (2H, dt, *J* = 6.0, 1.0 Hz), 3.30 (1H, m), 3.62 (1H, m), 3.70 (1H, dd, *J* = 11.5, 2.5 Hz), 4.05 (1H, ddd, *J* = 11.5, 3.5, 1.5 Hz), 5.28 (2H, m), 6.80 (1H, t, *J* = 5.5 Hz), 8.04 (1H, s), 8.25 (1H, s). 4 M HCl in dioxane (0.1 mL, 0.40 mmol) was added to a suspension of a portion of the carbamate (0.020 g, 0.06 mmol) in CH_2Cl_2 (1 mL), and the mixture was stirred at rt for 4.5 h. The suspension was then dissolved in MeOH and loaded onto an MP-TsOH resin cartridge (500 mg). The cartridge was washed with MeOH, and the product was eluted with 2 M ammonia in MeOH. The solvent was removed in vacuo to afford (4-(9*H*-purin-6-yl)morpholin-2-yl)methanamine (**10**) (0.013 g, 0.06 mmol, 93%). LC−MS *m*/*z* 235 (M + H^+), R_t = 0.68 min. Hi-Res LC−MS calcd for $C_{10}H_{15}N_6O$, 235.13019, found 235.13017 (M + H^+). ^{1}H NMR (MeOH-d_4) δ 2.77−2.88 (2H, m), 3.05 (1H, dd, *J* = 13.0, 10.5 Hz), 3.30 (1H, m), 3.62 (1H, m), 3.73 (1H, ddd, *J* = 11.5, 11.5, 2.5 Hz), 4.08 (1H, ddd, = 11.5, 3.5, 1.5 Hz), 5.25 (2H, m), 8.05 (1H, s), 8.25 (1H, s).

Ethyl 4-(2-(Aminomethyl)morpholino)-1*H*-pyrazolo[3,4-*b*]-pyridine-5-carboxylate (11). A solution of *tert*-butyl morpholin-2-ylmethylcarbamate (0.134 g, 0.62 mmol), ethyl 4-chloro-1*H*-pyrazolo[3,4-*b*]pyridine-5-carboxylate,[42] (0.142 g, 0.63 mmol) and Et_3N (0.26 mL, 1.87 mmol) in *n*-BuOH (2.5 mL) was heated at 120 °C in a microwave reactor for 60 min. The mixture was cooled, and the yellow solid was collected by filtration, redissolved in EtOAc (15 mL), and washed with brine (10 mL) and water (10 mL). The organic layer was concentrated to give ethyl 4-(2-((*tert*-butoxycarbonylamino)methyl)morpholino)-1*H*-pyrazolo[3,4-*b*]pyridine-5-carboxylate as a yellow solid (0.11 g, 0.27 mmol, 44%). LC−MS *m*/*z* 406 (M + H^+), R_t = 4.12 min. ^{1}H NMR (500 MHz, DMSO-d_6) δ 1.30 (3H, t, *J* = 7.5 Hz), 1.40 (9H, s), 2.95−3.20 (4H, m), 3.54 (1H, d, *J* = 13 Hz), 3.60−3.75 (3H, m), 3.94 (1H, d, *J* = 11.5 Hz), 4.25 (2H, q, *J* = 7.5 Hz), 7.00 (1H, s, broad), 8.24 (1H, s), 8.52 (1H, s). A portion of the carbamate (0.028 g, 0.07 mmol) was dissolved in methanol (3 mL), and CF_3CO_2H (2 mL) was added. The solution was refluxed for 16 h. The mixture was concentrated and the residue was purified by ion exchange chromatography on SCX-II acidic resin (2 g) eluting with MeOH then 2 M NH_3−MeOH. The basic fractions were combined and concentrated to give **11** as a yellow oil (0.020 g, 0.065 mmol, 93%). LC−MS *m*/*z* 306 (M + H^+), R_t = 1.22 min. Hi-Res LC−MS calcd for $C_{19}H_{28}N_5O_5$ 406.2085, found 406.2097 (M + H^+). ^{1}H NMR (500 MHz, CD_3OD) δ 1.40 (3H, t, *J* = 7.5 Hz), 2.75−2.90 (2H, m), 3.25 (1H, dd, *J* = 10, 12.5 Hz), 3.45−3.55 (1H, m), 3.65 (1H, d, *J* = 12.5 Hz), 3.75 (1H, d, *J* = 11.5 Hz), 3.84−3.90 (2H, m), 4.05 (1H, d, *J* = 11 Hz), 4.30 (2H, q, *J* = 7.5 Hz), 8.28 (1H, s), 8.65 (1H, s).

(4-(5-Bromo-1*H*-pyrazolo[3,4-*b*]pyridin-4-yl)morpholin-2-yl)methanamine (12). A suspension of 5-bromo-1-(4-methoxybenzyl)-1*H*-pyrazolo[3,4-*b*]pyridin-4(7*H*)-one (**15**)[43] (0.10 g, 0.30 mmol) in $POCl_3$ (2.5 mL, 27 mmol) was heated at 110 °C for 3 h. The solution was cooled, and volatile components were removed by evaporation. The remaining syrup was poured into ice−water and extracted with EtOAc (3 × 20 mL). The combined organic layers were washed with brine, dried, and concentrated to give a crude mixture containing 5-bromo-4-chloro-1*H*-pyrazolo[3,4-*b*]pyridine as the major component. LC−MS *m*/*z* 232, 234 (M + H^+), R_t = 4.43 min, purity = 52%. The crude material was added to a solution of *tert*-butyl morpholin-2-ylmethylcarbamate (0.098 g, 0.45 mmol) and Et_3N (0.14 mL, 0.99 mmol) in *n*-BuOH (1.87 mL) and was heated at 100 °C for 18 h. The mixture was cooled, concentrated, and purified by preparative TLC, eluting with 5% MeOH−CH_2Cl_2 to give *tert*-butyl (4-(5-bromo-1*H*-pyrazolo [3,4-*b*]pyridin-4-yl)morpholin-2-yl)methylcarbamate as a yellow powder (0.066 g, 53% over two steps). LC−MS *m*/*z* 412,

414 (M + H$^+$), R_t = 4.60 min. ^{1}H NMR (500 MHz, $CDCl_3$) δ 1.47 (9H, s), 3.20 (1H, t, J = 11 Hz), 3.26−3.32 (1H, m), 3.37−3.56 (1H, m), 3.88−3.42 (2H, m), 3.82−3.86 (3H, m), 4.07 (1H, d, J = 11.5 Hz), 8.18 (1H, s), 8.48 (1H, s). A portion of the carbamate (0.033 g, 0.08 mmol) was dissolved in dioxane (0.5 mL), and 4 M HCl in dioxane (0.5 mL, 2.0 mmol) was added. The solution was stirred at rt for 18 h. The solution was concentrated, and the residue was dissolved in MeOH and purified by ion exchange chromatography on Isolute SCX II acidic resin (2 g), eluting with MeOH and then 1 M NH_3−MeOH. Preparative TLC, eluting with 1:20:79 Et_3N:MeOH:CH_2Cl_2, gave **12** as an off-white amorphous powder (0.002 g, 0.0064 mmol, 8%). LC−MS m/z 312, 314 (M + H$^+$), R_t = 1.63 min. Hi-Res LC−MS calcd for $C_{11}H_{15}BrN_5O$ 312.04545, found 312.04543 (M + H$^+$). ^{1}H NMR (500 MHz, MeOH-d_4) δ 2.85−2.93 (2H, m), 3.20 (1H, dt, J = 2.0, 10.0 Hz), 3.41−3.46 (1H, m), 3.81−3.86 (2H, m), 3.89−3.94 (2H, m), 4.10−4.13 (1H, m), 8.29 (1H, s), 8.40 (1H, s).

(4-(5-(Thiophen-3-yl)-1*H*-pyrazolo[3,4-*b*]pyridin-4-yl)morpholin-2-yl)methanamine (13). A suspension of **15**[43] (0.20 mg, 0.60 mmol) in $POCl_3$ (5 mL, 54 mmol) was heated at 60 °C for 18 h. The mixture was cooled, and volatile components were removed by evaporation. The remaining syrup was poured into ice−water and extracted with EtOAc (3 × 20 mL). The combined extracts were washed with brine, dried, and concentrated to give 5-bromo-4-chloro-1-(4-methoxybenzyl)-1*H*-pyrazolo[3,4-*b*]pyridine as an off-white amorphous powder (0.166 g, 0.47 mmol, 79%). LC−MS m/z 352, 354 (M + H$^+$), R_t = 5.70 min, purity = 91%. ^{1}H NMR (500 MHz, MeOH-d_4) δ 3.70 (3H, s), 5.61 (2H, s), 6.86 (2H, d, J = 8.5 Hz), 7.22 (2H, d, J = 8.5 Hz), 8.29 (1H, s), 8.79 (1H, s). A portion of the material (0.10 g, 0.28 mmol) was dissolved in warmed *n*-BuOH (1.2 mL), and *tert*-butyl morpholin-2-ylmethylcarbamate (0.135 g, 0.62 mmol) and Et_3N (0.18 mL, 1.31 mmol) were added. The reaction mixture was heated in a microwave reactor at 160 °C for 3 h. The mixture was cooled and concentrated. Flash column chromatography on silica, eluting with a gradient of EtOAc−hexanes, gave **16** as a white amorphous powder (0.074 g, 49%). LC−MS m/z 532, 534 (M + H$^+$), R_t = 5.49 min. ^{1}H NMR (500 MHz, MeOH-d_4) δ 1.45 (9H, s), 3.11−3.15 (1H, m), 3.19−3.27 (2H, m), 3.36−3.41 (1H, m), 3.52−3.59 (1H, m), 3.73 (3H, s), 3.77−3.94 (3H, m), 4.03−4.05 (1H, m), 5.54 (2H, s), 6.82 (2H, d, J = 8.5 Hz), 7.22 (2H, d, J = 8.5 Hz), 8.24 (1H, s), 8.42 (1H, s). A portion of **16** (16 mg, 0.030 mmol) was dissolved in warmed MeCN (0.56 mL) before 3-thienylboronic acid (8 mg, 0.060 mmol), Na_2CO_3 (8 mg, 0.075 mmol), Pd(dppf)·CH_2Cl_2 complex (2.2 mg, 10 mol %), and water (0.11 mL) were added. The reaction vial was capped and purged with N_2 for 5 min. The reaction mixture was heated in a microwave reactor at 140 °C for 30 min. The cooled solution was filtered through celite, washing with fresh MeCN and MeOH. The organic filtrates were combined and the volatiles were removed in vacuo to give crude *tert*-butyl (4-(1-(4-methoxybenzyl)-5-(thiophen-3-yl)-1*H*-pyrazolo[3,4-*b*]pyridin-4-yl)morpholin-2-yl)methylcarbamate. LC−MS m/z 536 (M + H$^+$); R_t = 5.47 min, 58% purity. The crude material was dissolved in CF_3CO_2H (1 mL) and stirred at 40 °C under N_2 for 18 h. The solution was concentrated, and the residue was dissolved in DMF/MeOH before ion exchange chromatography on Isolute SCX II acidic resin (2 g), eluting with MeOH and then 1 M NH_3−MeOH. Preparative TLC, eluting with 1:10:89 NH_3:MeOH:CH_2Cl_2, gave **13** as a white amorphous powder (3.9 mg, 41% over 2 steps). LC−MS m/z 316 (M + H$^+$), R_t = 0.93 min. Hi-Res LC−MS calcd for $C_{15}H_{18}N_5OS$ 316.12266, found 316.12310 (M + H)$^+$. ^{1}H NMR (500 MHz, MeOH-d_4) δ, 2.65−2.75 (2H, m), 2.97 (1H, dd, J = 10.0, 12.0), 3.24 (1H, td, J = 3.2, 12.1), 3.47−3.52 (1H, m), 3.58 (1H, dt, J = 2.0, 12.0), 3.60−3.66 (2H, m), 3.70 (1H, td, J = 2.5, 11.5), 3.89 (1H, ddd, J = 1.5, 3.0, 11.5), 7.40 (1H, dd, J = 1.5, 5.0), 7.52 (1H, dd, J = 1.5, 3.0), 7.57 (1H, dd, J = 3.0, 5.0), 8.20 (s, 1H), 8.32 (s, 1H),

(4-(5-Phenyl-1*H*-pyrazolo[3,4-*b*]pyridin-4-yl)morpholin-2-yl)methanamine (14). (16% over two steps from **16**). LC−MS m/z 310 (M + H$^+$), R_t = 0.67 min. Hi-Res LC−MS calcd for $C_{17}H_{19}N_5O$ 310.16624, found 310.16629 (M + H$^+$). ^{1}H NMR (500 MHz, MeOH-d_4) δ 2.89−2.95 (2H, m), 3.05 (1H, dd, J = 10.0, 12.0 Hz), 3.20−3.26 (1H, m), 3.47−3.49 (1H, m), 3.60−3.65 (1H, m), 3.74−3.79 (1H, m), 3.86−3.89 (1H, m), 7.37−7.41 (1H, m), 7.51 (2H, t, J = 7.5 Hz), 7.56 (2H, dd, J = 1.5, 7.5 Hz), 8.14 (1H, s), 8.32 (1H, s).

Acknowledgment. We thank Dr. N. Proisy for initial synthetic work in the preparation of **18** and Dr. A. Mirza and M. Richards for assistance in the spectroscopic characterisation of test compounds. This work was supported by Cancer Research UK [CUK] grant numbers C309/A2187, C309/A8274 and C309/A8365. We acknowledge NHS funding to the NIHR Biomedical Research Centre.

Supporting Information Available: Experimental procedures for the preparation of compounds **19**, **20**, **21**, (***R***)-**14**, and (***S***)-**14**. Experimental procedures and CHK1 inhibitory data for the preparation of additional analogues related to compounds **9** and **10**. Methods for high concentration CHK1 AlphaScreen, DELFIA enzyme inhibition assays for CHK1, CHK2, and CDK1, G2 checkpoint abrogation assay, SRB cytotoxicity assay. Methods for crystal structure determination of CHK1−inhibitor complexes, crystallographic information on the structures of **5**−**10**, **12**, **14**. This material is available free of charge via the Internet at http://pubs.acs.org.

References

(1) Walworth, N. Cell-cycle checkpoint kinases: checking in on the cell cycle. *Curr. Opin. Cell Biol.* **2000**, *12*, 697–704.
(2) Bartek, J.; Lukas, J. Chk1 and Chk2 kinases in checkpoint control and cancer. *Cancer Cell* **2003**, *3*, 421–429.
(3) Luo, Y.; Leverson, J. D. New opportunities in chemosensitization and radiosensitization: modulating the DNA-damage response. *Expert Rev. Anticancer Ther.* **2005**, *5*, 333–342.
(4) Bourdon, J.-C. p53 and its isoforms in cancer. *Br. J. Cancer* **2007**, *97*, 277–282.
(5) Chen, Z.; Xiao, Z.; Chen, J.; Ng, S. C.; Sowin, T.; Sham, H.; Rosenberg, S.; Fesik, S.; Zhang, H. Human Chk1 expression is dispensable for somatic cell death and critical for sustaining G2 DNA damage checkpoint. *Mol. Cancer Ther.* **2003**, *2*, 543–548.
(6) Bucher, N.; Britten, C. D. G2 checkpoint abrogation and checkpoint kinase-1 targeting in the treatment of cancer. *Br. J. Cancer* **2008**, *98*, 523–528.
(7) Chen, Z.; Xiao, X.; Gu, W.; Xue, J.; Bui, M. H.; Kovar, P.; Li, G.; Wang, G.; Tao, Z.-F.; Tong, Y.; Lin, N.-H.; Sham, H. L.; Wang, J. Y. J.; Sowin, T. J.; Rosenberg, S. H.; Zhang, H. Selective Chk1 inhibitors differentially sensitize p53-deficient cells to cancer therapeutics. *Int. J. Cancer* **2006**, *119*, 2784–2794.
(8) Zhou, B. B.; Bartek, J. Targeting the checkpoint kinases: chemosensitization versus chemoprotection. *Nat. Rev. Cancer* **2004**, *4*, 216–225.
(9) Tse, A. N.; Carvajal, R.; Scwartz, G. K. Targeting checkpoint kinase 1 in cancer therapeutics. *Clin. Cancer Res.* **2007**, *13*, 1955–1960.
(10) Lam, M. H.; Rosen, J. M. Chk1 versus Cdc25: chking one's levels of cellular proliferation. *Cell Cycle* **2004**, *3*, 1355–1357.
(11) Xiao, Z.; Xue, J.; Sowin, T. J.; Zhang, H. Differential roles of checkpoint kinase 1, checkpoint kinase 2, and mitogen-activated protein kinase-activated protein kinase 2 in mediating DNA damage-induced cell cycle arrest: implications for cancer therapy. *Mol. Cancer Ther.* **2006**, *5*, 1935–1943.
(12) Ganzeinelli, M.; Carrassa, L.; Crippa, F.; Tavecchio, M.; Broggini, M.; Damia, G. Checkpoint kinase 1 down-regulation by an inducible small interfering RNA expression system sensitized in vivo tumours to treatment with 5-fluorouracil. *Clin. Cancer Res.* **2008**, *14*, 5131–5141.
(13) Collins, I.; Garrett, M. Inhibitors of the cell cycle. *Curr. Opin. Pharmacol.* **2005**, *5*, 366–373.
(14) Tao, Z.-F.; Lin, N.-H. Chk1 inhibitors for novel cancer treatment. *Anticancer Agents Med. Chem.* **2006**, *6*, 377–388.
(15) (a) Wang, G. T.; Li, G.; Mantei, R. A.; Chen, Z.; Kovar, P.; Gu, W.; Xiao, Z.; Zhang, H.; Sham, H. L.; Sowin, T.; Rosenberg, S. H.; Lin, N.-H. 1-(5-Chloro-2-alkoxyphenyl)-3-(5-cyanopyrazin-2-yl)ureas

as potent and selective inhibitors of Chk1 kinase: synthesis, preliminary SAR, and biological activities. *J. Med. Chem.* **2005**, *48*, 31118–3121. (b) Tong, Y.; Claiborne, A.; Stewart, K. D.; Park, C.; Kovar, P.; Chen, Z.; Credo, R. B.; Gu, W.-Z.; Gwaltney, S. L.II; Judge, R. A.; Zhang, H.; Rosenberg, S. H.; Sham, H. L.; Sowin, T. J.; Lin, N. Discovery of 1,4-dihydroindeno[1,2-c]pyrazoles as a novel class of potent and selective checkpoint kinase 1 inhibitors. *Bioorg. Med. Chem.* **2007**, *15*, 2759–2767. (c) Wang, L.; Sullivan, G. M.; Hexamer, L. A.; Hasvold, R. T.; Przytulinska, M.; Tao, Z.-F.; Li, G.; Chen, Z.; Xiao, Z.; Gu, W.-Z.; Xue, J.; Bui, M.-H.; Merta, P.; Kovar, P.; Bouska, J. J.; Zhang, H.; Park, C.; Stewart, K. D.; Sham, H. L.; Sowin, T. J.; Rosenberg, S. H.; Lin, N.-H. Design, synthesis and biological activity of 5,10-dihydro-dibenzo[b,e][1,4]diazepin-11-one-based potent and selective Chk-1 inhibitors. *J. Med. Chem.* **2007**, *50*, 4162–4176.

(16) (a) Huang, S.; Garbaccio, R. M.; Fraley, M. E.; Steen, J.; Kreatsoulas, C.; Hartmann, G.; Stirdivant, S.; Drakas, B.; Rickert, K.; Walsh, E.; Hamilton, K.; Buser, C. A.; Hardwick, J.; Mao, X.; Abrams, M.; Beck, S.; Tao, W.; Lobell, R.; Sepp-Lorenzino, L.; Yan, Y.; Ikuta, M.; Murphy, J. Z.; Sardana, V.; Munshi, S.; Kuo, L.; Reilly, M.; Mahan, E. Development of 6-substituted indolylquinolinones as potent Chek1 inhibitors. *Bioorg. Med. Chem. Lett.* **2006**, *16*, 5907–5912. (b) Fraley, M. E.; Steen, J. T.; Brnardic, E. J.; Arrington, K. L.; Spencer, K. L.; Hanney, B. A.; Kim, Y.; Hartman, G. D.; Stirdivant, S. M.; Drakas, B. A.; Rickert, K.; Walsh, E. S.; Hamilton, K.; Buser, C. A.; Hardwick, J.; Tao, W.; Beck, S. C.; Mao, X.; Lobell, R. B.; Sepp-Lorenzino, L.; Yan, Y.; Ikuta, M.; Munshi, S. K.; Kuo, L. C.; Kreatsoulas, C. 3-(Indol-2-yl)indazoles as Chek1 kinase inhibitors: Optimization of potency and selectivity via substitution at C6. *Bioorg. Med. Chem. Lett.* **2006**, *16*, 6049–6053.

(17) Teng, M.; Zhu, J.; Johnson, M. D.; Chen, P.; Kornmann, J.; Chen, E.; Blasina, A.; Register, J.; Anderes, K.; Rogers, C.; Deng, Y.; Ninkovic, S.; Grant, S.; Hu, Q.; Lundgren, K.; Peng, Z.; Kania, R. S. Structure-based design and synthesis of (5-arylamino-2*H*-pyrazol-3-yl)-biphenyl-2′,4′-diols as novel and potent human CHK1 inhibitors. *J. Med. Chem.* **2007**, *50*, 5253–5256.

(18) Tse, A.; Rendahl, K. G.; Sheikh, T.; Cheema, H.; Aardalen, K.; Embry, M.; Ma, S.; Moler, E. J.; Nie, Z. J.; Lopas de Menezes, D. E.; Hibner, B.; Gesner, T. G.; Schwartz, G. K. CHIR-124, a novel potent inhibitor of Chk1, potentiates the cytotoxicity of topoisomerase 1 poisons in vitro and in vivo. *Clin. Cancer Res.* **2007**, *13*, 591−602.

(19) Blasina, A.; Hallin, J.; Chen, E.; Arango, M. E.; Kraynov, E.; Register, J.; Gant, S.; Ninkovic, S.; Chen, P.; Nichols, T.; O'Connor, P.; Anderes, K. Breaching the DNA damage checkpoint with PF-00477736, a novel small-molecule inhibitor of checkpoint kinase 1. *Mol. Cancer Ther.* **2008**, *7*, 2394–2404.

(20) Zabludoff, S. D.; Deng, C.; Grondine, M. R.; Sheehy, A. M.; Ashwell, S.; Caleb, B. L.; Green, S.; Haye, H. R.; Horn, C. L.; Janetka, J. W.; Liu, D.; Mouchet, E.; Ready, S.; Rosenthal, J. L.; Queva, C.; Schwartz, G. K.; Taylor, K. J.; Tse, A. N.; Walker, G. E.; White, A. M. AZD7762, a novel checkpoint kinase inhibitor, drives checkpoint abrogation and potentiates DNA-targeted therapies. *Mol. Cancer Ther.* **2008**, *7*, 2955–2966.

(21) Ashwell, S.; Zabludoff, S. DNA damage detection and repair pathways−recent advances with inhibitors of checkpoint kinases in cancer therapy. *Mol. Cancer Ther.* **2008**, *14*, 4032–4037.

(22) Janetka, J. W.; Ashwell, S.; Zabludoff, S.; Lyne, P. Inhibitors of checkpoint kinases: from discovery to the clinic. *Curr. Opin. Drug Discovery Dev.* **2007**, *10*, 473–486.

(23) Prudhomme, M. Novel CHK1 inhibitors. *Recent Pat. Anti-Cancer Drug Discovery* **2006**, *1*, 55–68.

(24) Hénon, H.; Conchon, E.; Hugon, B.; Messaoudi, S.; Golsteyn, R. M.; Prudhomme, M. Pyrrolocarbazoles as checkpoint 1 kinase inhibitors. *Anticancer Agents Med. Chem.* **2008**, *8*, 577–597.

(25) Lyne, P. D.; Kenny, P. W.; Cosgrove, D. A.; Deng, C.; Zabludoff, S.; Wendeloski, J. J.; Ashwell, S. Identification of compounds with nanomolar binding affinity for checkpoint kinase-1 using knowledge-based virtual screening. *J. Med. Chem.* **2004**, *47*, 1962–1968.

(26) Foloppe, N.; Fisher, L .M.; Howes, R.; Potter, A.; Robertson, A. G. S.; Surgenor, A. E. Identification of chemically diverse Chk1 inhibitors by receptor-based virtual screening. *Bioorg. Med. Chem.* **2006**, *14*, 4792–4802.

(27) Chen, P.; Luo, C.; Deng, Y.; Ryan, K.; Register, J.; Margosiak, S.; Tempczyk-Russell, A.; Nguyen, B.; Myers, P.; Lundgren, K.; Kan, C.-C.; O'Connor, P. M. The 1.7 A crystal structure of human cell cycle checkpoint kinase Chk1: implications for Chk1 regulation. *Cell* **2000**, *100*, 681–692.

(28) Jhoti, H.; Cleasby, A.; Verdonk, M.; Williams, G. Fragment-based screening using X-ray crystallography and NMR spectroscopy. *Curr. Opin. Chem. Biol.* **2007**, *11*, 485–493.

(29) Hopkins, A. L.; Groom, C. R.; Alex, A. Ligand efficiency: a useful metric for lead selection. *Drug Discovery Today* **2004**, *9*, 430–431.

(30) Card, G. L.; Blasdel, L.; England, B. P.; Zhang, C.; Suzuki, Y.; Gillette, S.; Fong, D.; Ibrahim, P. N.; Artis, D. R.; Bollag, G.; Milburn, M. V.; Kim, S. H.; Schlessinger, J.; Zhang, K. Y. A family of phosphodiesterase inhibitors discovered by cocrystallography and scaffold-based drug design. *Nat. Biotechnol.* **2005**, *23*, 184–186.

(31) Collins, I.; Workman, P. New approaches to molecular cancer therapeutics. *Nat. Chem. Biol.* **2006**, *2*, 689–700.

(32) *Chemical Computing Group*; http://www.chemcomp.com. Accessed on 24 June 2009.

(33) Von Leoprechting, A.; Kumpf, R.; Menzel, S.; Reulle, D.; Griebel, R.; Valler, M. J.; Buttner, F. H. Miniaturization and validation of a high-throughput serine kinase assay using the AlphaScreen platform. *J. Biomol. Screen.* **2004**, *9*, 719–725.

(34) Ryan, A. J.; Gray, N. M.; Lowe, P. N.; Chung, C. W. Effect of detergent on "promiscuous" inhibitors. *J. Med. Chem.* **2003**, *46*, 3448–3451.

(35) Burns, S.; Travers, J.; Collins, I.; Rowlands, M. G.; Newbatt, Y.; Thompson, N.; Garrett, M. D.; Workman, P.; Aherne, W. Identification of small molecule inhibitors of protein kinase B (PKB) in an AlphaScreen high-throughput screen. *J. Biomol. Screening* **2006**, *11*, 822–827.

(36) Babaoglu, K.; Shoichet, B. K. Deconstructing fragment-based inhibitor discovery. *Nat. Chem. Biol.* **2006**, *2*, 658–659.

(37) Foloppe, N.; Fisher, L. M.; Francis, G.; Howes, R.; Kierstan, P.; Potter, A. Identification of a buried pocket for potent and selective inhibition of CHk1: Prediction and verification. *Bioorg. Med. Chem.* **2006**, *14*, 1792–1804.

(38) (a) Gibson, A. E.; Arris, C. E.; Bentley, J.; Boyle, F. T.; Curtin, N. J.; Davies, T. G.; Endicott, J. A.; Golding, B. T.; Grant, S.; Griffin, R. J.; Jewsbury, P.; Johnson, L. N.; Mesguiche, V.; Newell, D. R.; Noble, M. E.; Tucker, J. A.; Whitfield, H. J. Probing the ATP ribose-binding domain of cyclin-dependent kinases 1 and 2 with O (6)-substituted guanine derivatives. *J. Med. Chem.* **2002**, *45*, 3381–3393. (b) Hardcastle, I. R.; Arris, C. E.; Bentley, J.; Boyle, F. T.; Chen, Y.; Curtin, N. J.; Endicott, J. A.; Gibson, A. E.; Golding, B. T.; Griffin, R. J.; Jewsbury, P.; Menyerol, J.; Mesguiche, V.; Newell, D. R.; Noble, M. E.; Pratt, D. J.; Wang, L. Z.; Whitfield, H. J. N2-substituted O6-cyclohexylmethylguanine derivatives: potent inhibitors of cyclin-dependent kinases 1 and 2. *J. Med. Chem.* **2004**, *47*, 3710–3722.

(39) (a) Donald, A.; McHardy, T.; Rowlands, M. G.; Hunter, L. K.; Davies, T. G.; Boyle, R. G.; Aherne, G. W.; Garrett, M. D.; Collins, I. Rapid evolution of 6-phenylpurine inhibitors of protein kinase B through structure-based design. *J. Med. Chem.* **2007**, *50*, 2289–2293. (b) Caldwell, J. J.; Davies, T. G.; Donald, A.; McHardy, T.; Rowlands, M. G.; Aherne, G. W.; Hunter, L. K.; Taylor, K.; Ruddle, R.; Raynaud, F. I.; Verdonk, M.; Workman, P.; Garrett, M. D.; Collins, I. Identification of 4-(4-aminopiperidin-1-yl)-7H-pyrrolo[2,3-d]pyrimidines as selective inhibitors of protein kinase B through fragment elaboration. *J. Med. Chem.* **2008**, *51*, 2147–2157.

(40) Shapiro, G. I. Cyclin-dependent kinase pathways as targets for cancer treatment. *J. Clin. Oncol.* **2006**, *24*, 1770–1783.

(41) Xiao, Z.; Xue, J.; Gu, W.-Z.; Bui, M.; Li, G.; Tao, Z.-F.; Lin, N.-H.; Sowin, T. J.; Zhang, H. Cyclin B1 is an efficacy-predicting biomarker for Chk1 inhibitors. *Biomarkers* **2008**, *13*, 579–596.

(42) Hoehn, H.; Denzel, T. 1*H*-Pyrazolo[3,4-*b*]pyridines. Patent Appl. DE2301268, **1973** ; *Chem. Abs.* **1973**, *79*, 115578.

(43) Misra, R. N.; Xiao, H.-Y.; Rawlins, D. B.; Shan, W.; Kellar, K. A.; Mulheron, J. G.; Sack, J. S.; Tokarski, J. S.; Kimball, S. D.; Webster, K. R. 1*H*-Pyrazolo[3,4-*b*]pyridine inhibitors of cyclin-dependent kinases: highly potent 2,6-difluorophenacyl analogues. *Bioorg. Med. Chem. Lett.* **2003**, *13*, 2405–2408.

(44) Brenner, E.; Baldwin, R. M.; Tamagnan, G. Asymmetric synthesis of (+)-(*S*,*S*)-reboxetine via a new (*S*)-2-(hydroxymethyl)morpholine preparation. *Org. Lett.* **2005**, *7*, 937–939.

(45) Parry, D.; Shanahan, F.; Davis, N.; Wiswell, D.; Seghezzi, W.; Pierce, R.; Hsieh, Y.; Paruch, K.; Guzi, T. Targeting the replication checkpoint with a potent and selective CHK1 inhibitor SCH 900776. Abstracts of the 100th AACR Annual Meeting, Denver, CO, April 18−29, 2009, paper 2490.

(46) (a) Schirok, H.; Kast, R.; Figueroa-Perez, S.; Bennabi, S.; Gnoth, M. J.; Feurer, A.; Heckroth, H.; Thutewohl, M.; Paulsen, H.; Knorr, A.; Huetter, J.; Lobell, M.; Muenter, K.; Geiss, V.; Ehmke, H.; Lang, D.; Radtke, M.; Mittendorf, J.; Stasch, J. Design and synthesis of potent and selective azaindole-based Rho kinase (ROCK) inhibitors. *ChemMedChem* **2008**, *3*, 1893–1904. (b) Dai, Y.; Hartandi, K.; Soni, N. B.; Pease, L. J.; Reuter, D. R.; Olson, A. M.; Osterling, D. J.; Doktor, S. Z.; Albert, D. H.; Bouska, J. J.; Glaser, K. B.; Marcotte, P. A.; Stewart, K. D.; Davidsen, S. K.; Michaelides, M. R. Identification of aminopyrazolopyridine ureas as potent VEGFR/PDGFR multitargeted kinase inhibitors. *Bioorg. Med. Chem. Lett.* **2008**, *18*, 386–390. (c) Lin, R.; Connolly, P. J.; Lu, Y.; Chiu, G.; Li, S.; Yu, Y.; Huang, S.; Li, X.; Emanuel, S. L.; Middleton, S. A.; Gruninger, R. H.; Adams, M.; Fuentes-Pesquera, A. R.; Greenberger, L. M.

Synthesis and evaluation of pyrazolo[3,4-b]pyridine CDK1 inhibitors as antitumor agents. *Bioorg. Med. Chem. Lett.* **2007**, *17*, 4297–4302. (d) Witherington, J.; Bordas, V.; Gaiba, A.; Garton, N. S.; Naylor, A.; Rawlings, A. D.; Slingsby, B. P.; Smith, D. G.; Takle, A. K.; Ward, R. W. 6-Aryl-pyrazolo[3,4-b]pyridines: potent inhibitors of glycogen synthase kinase-3 (GSK-3). *Bioorg. Med. Chem. Lett.* **2003**, *13*, 3055–3057. (e) Witherington, J.; Bordas, V.; Garland, S. L.; Hickey, D. M. B.; Ife, R. J.; Liddle, J.; Saunders, M.; Smith, D. G.; Ward, R. W. 5-Aryl-pyrazolo[3,4-b]pyridines: potent inhibitors of glycogen synthase kinase-3 (GSK-3). *Bioorg. Med. Chem. Lett.* **2003**, *13*, 1577–1580. (f) Misra, R. N.; Rawlins, D. B.; Xiao, H.; Shan, W.; Bursuker, I.; Kellar, K. A.; Mulheron, J. G.; Sack, J. S.; Tokarski, J. S.; Kimball, S. D.; Webster, K. R. 1H-Pyrazolo[3,4-b]pyridine inhibitors of cyclin-dependent kinases. *Bioorg. Med. Chem. Lett.* **2003**, *13*, 1133–1136.

(47) Collins, I.; Reader, J. C.; Cheung, K. M.; Matthews, T. P.; Proisy, N.; Klair, S. S. Patent Appl. WO2008075007, **2008**; *Chem. Abstr.* **2008**, *149*, 104737.